Journal of Drug Delivery Science and Technology 80 (2023) 104148

Contents lists available at ScienceDirect

Journal of Drug Delivery Science and Technology

journal homepage: www.elsevier.com/locate/jddst

EGF-conjugated bio-safe luteolin gold nanoparticles induce cellular toxicity and cell death mediated by site-specific rapid uptake in human triple negative breast cancer cells

Suvadeep Mal [a,b], Tiyasa Saha [c], Asim Halder [a], Sudhir Kumar Paidesetty [b], Suvadra Das [d], Wong Tin Wui [e], Urmi Chatterji [c], Partha Roy [a,*]

[a] Department of Pharmaceutical Technology, Adamas University, Barasat-Barrackpore Road, Kolkata, 700126, India
[b] Department of Pharmaceutical Chemistry, Siksha 'O' Anusandhan University (Deemed to be University), Campus-2, Ghatikia, Kalinga Nagar, Bhubaneswar, 731003, Odisha, India
[c] Cancer Research Lab, Department of Zoology, University of Calcutta, 35, Ballygunge Circular Road, Kolkata, 700019, India
[d] Basic Science and Humanities Department, University of Engineering and Management, University Area, Plot, Street Number 03, Action Area III, B/5, Newtown, Kolkata, West Bengal, 700156, India
[e] Non-Destructive Biomedical and Pharmaceutical Research Centre, Smart Manufacturing Research Institute, Universiti Teknologi MARA, Selangor, Malaysia

ARTICLE INFO

Keywords:
Triple negative breast cancer
Biosafe gold nanoparticles
Luteolin
Cell death
Epidermal growth factor receptor

ABSTRACT

World Health Organization listed breast cancer as the most prevalent form of cancer in recent times. Triple negative breast cancer is its deadliest sub-type characterized by high rate of metastasis and poor prognosis, as it lacks three important therapeutic targets like progesterone, estrogen and HER-2 receptors. This fatal variant exhibit over-expressed epidermal growth factor receptor in 45–70% of infected patients. The present work explores a strategy to target this receptor with flavonoid (luteolin)-conjugated gold nanoparticles synthesized through a facile and fast ultra-sonication assisted route. Synthesized nanoparticles exhibited a diameter of 30.23 ± 9.96 nm in TEM and possessed high stability as suggested from zeta potential of −38.1 ± 1.49 mV. The particles showed a characteristic plasmonic resonance at 541 nm measured in UV–Vis spectroscopy. Spherical particles with face centered cubic crystalline structure were observed through HR-TEM, SAED and XRD analysis. Synthesized nanoparticles exhibited significant cytotoxicity (IC_{50} value of 2 μg/mL) and induced cell death in MDA-MB-231 TNBC cells. Confocal microscopy confirmed rapid localization of targeted nanoparticles in the nucleus of cancer cells leading to its improved performance. Cell cycle and apoptosis evaluations divulged the occurrence of both necrotic and apoptotic cell death following accumulation of MDA-MB-231 cells in sub-G_1 phases. Interestingly nanoparticles were cytocompatible with non-malignant NIH-3T3 cells supporting its clinical promise as a biosafe formulation. The work reflects the first report of Luteolin-conjugated bio-safe gold nanoparticles as targeted therapeutics against triple negative breast cancer.

1. Introduction

World Health Organization reports cancer as the forerunner among mortality causes for individuals around 70 years of age in 112 countries [1]. Global socioeconomic transformation with overlapping stress initiators remains as the main impetus behind rising cancer incidences across geographical frontiers. Out of diverse cancer types, female breast cancer (BC) has emerged as the most commonly detected and rapidly spreading variant although it is predominantly gender specific [2]. Triple negative breast cancer (TNBC) is an extremely intrusive variant of BC and is prominent in approximately 20% of all BC cases [3,4]. Moreover, the disease offers poor prognosis with increased risk of relapse after conventional chemotherapy. TNBC also leads to metastasis of the lung, liver and brain and presents leads the highest death rate among all other breast cancer types [5]. Prevalent treatment strategy for TNBC is combination of chemotherapy, surgery and radiation depending on the patient condition [6].

Flavonoids are plant derived chemo-preventives present in a wide array of fruits and vegetables with reported success in TNBC [7]. Luteolin (Lu) is a natural 3′, 4′, 5, 7-tetrahydroxyflavone linked to

* Corresponding author.
E-mail address: partharoy2502@gmail.com (P. Roy).

https://doi.org/10.1016/j.jddst.2022.104148
Received 21 July 2022; Received in revised form 29 December 2022; Accepted 31 December 2022
Available online 31 December 2022
1773-2247/

management of diverse cancers like liver, skin, stomach, prostrate, pancreas, ovary and colon [8,9]. The flavonoid structure reveals a three-ring assembly with two benzene rings and a heterocyclic ring (3, 4-dihydro-2*H*-pyran) with oxygen where the C2–C3 double bond and C3' and C4' hydroxyl groups are mostly linked to its biological activity [10]. However, problems like poor solubility and bioavailability hinders its easy passage to the clinic [11].

Spotlight on the etiology of TNBC related mortality confirms tumor metastasis and ancillary tumor growth at migrated sites as the predominant causes. Adding to the complexity, clinical strategy for TNBC management often involves non-targeted chemotherapeutic regimens leading to toxic outcomes, as the cancer variant lacks suitable drug targets like Estrogen Receptor (ER), Progesterone Receptor (PR), and Human Epidermal Growth Factor Receptor (HER2) [12]. Hyperactive Wnt/β-catenin pathway elevates the expression of transcriptional factors like Snail and Slug, which induces EMT (Epithelial-to-Mesenchymal Transition), responsible for metastasis of TNBC cells [13,14]. It is reported that Lu helps in blocking metastasis of TNBC cells to the brain by reversing EMT along with down regulating the Wnt/β-catenin pathway [15]. Lu is also reported to be effective for management of both early-stage and late-stage TNBC by suppressing angiogenesis and metastasis [16]. Another study reports the capability of Lu to arrest cell cycle at the S and G2/M phases by suppressing ^{3}H-thymidine incorporation along with apoptotic activity by decreasing several down-stream pathways e.g. AKT, or by hampering the gene (PLK1, cyclin A, cyclin B1, CDC2, CDK2, *Bcl-XL*) expressions and increasing pro-apoptotic p21 and *Bax* expression in TNBC [17].

PEGylated gold nanoparticles, on the other hand, is reported to be cytotoxic to basal-like TNBC cells in a dose-dependent manner [18]. Some researchers reported that gold nanoparticle influenced TNBC cytotoxicity and is associated with diverse epigenetic modifications which vary with the surface charge of the nanoparticles. Additionally, these nanoparticles are reported to enhance sensitivity of TNBC cells to chemotherapeutics like 5-Flurouracil by modulating thymidylate synthase manifestations [19]. In another study with bifunctional theranostic gold nanoprobes, selective cytotoxicity to TNBC cells by alterations of ROS levels was observed keeping the normal cells remained unaffected [20]. It was reported that Lu has the reduction potential of 0.23 V with two metal ion-chelating sites, which assist to target metals and scavenge free radicals [21]. Our synthetic strategy thus aimed to explore a novel, eco-friendly and cost-effective approach for the reduction of Au^{3+} to Au^{0} where the flavonoid plays the dual role of reducing and capping agent. Therefore, improved biological activity against TNBC cells with relatively cyto-compatibility towards normal cells was anticipated due to Lu association with nano-scale gold.

One of the main reasons for the failure in drug development strategy in order to overcome TNBC is the absence of molecular targets, which instigates further mining for novel therapies and strategies. Several TNBC cell lines, like MDA-MB-231 and MDA-MB-468, show frequent and upraised expression of the Epidermal Growth Factor Receptor [EGFR] [22]. In fact, EGFR overexpression has been found in 45–70% of cases of TNBC, which is the highest among other breast cancer subtypes [23,24]. Though HER2 remains absent in TNBC, the gene amplification and specific translation of this gene (*HER-2*) by RNA is linked with the overexpression of EGFR (a HER family subtype, HER1) [25,26]. Elevated occurrence of EGFR in TNBC makes it a promising target in the clinical management of TNBC. Keeping this in mind, we conjugated EGF with the flavonoid derived nano-scale gold to achieve the site specificity to TNBC's. Present work marks the first report of Lu conjugated gold nanoparticles (LuAunp) as targeted therapeutics in TNBC management.

2. Materials and methods

2.1. Materials

Chloroauric acid ($HAuCl_4$, $3H_2O$), and 1-Ethyl-3-[3-dimethylaminopropyl]carbodiimide hydrochloride (EDC) were procured from Alfa Aesar (Haverhill, Massachusetts, United States). 3′,4′,5,7-tetrahydroxyflavone (Luteolin, Lu), *N*-hydroxysuccinimide (NHS) were purchased from TCI (Tokyo, Japan). FTIR grade KBr was purchased from Merck (Burlington, Massachusetts, United States). Human triple negative breast cancer (TNBC) cell line, MDA-MB-231 and mouse fibroblast cell line, NIH/3T3 were procured from the National Centre for Cell Sciences (Pune, India). Fetal bovine serum (FBS), Dulbecco's Modified Eagle Medium (DMEM), and antibiotic-antimycotic mix were obtained from Himedia (India). EGF (epidermal growth factor-human), MTT (3-(4,5-dimethylthiazol-2-yl)-2,5-diphenyl tetrazolium bromide), Annexin V-FITC Early Apoptosis Detection Kit, 4′,6-diamidino-2-phenylindole (DAPI), propidium iodide (PI) and Triton X-100 were procured from Sigma Aldrich (St. Louis, MO, USA). Paraformaldehyde, phosphate buffer saline (PBS) and RNaseA were acquired from MERCK (USA). ProLong™ antifade reagent was procured from Thermo Fisher (USA).

HPLC grade solvents procured from Spectrochem (Mumbai, India) was used for the entire experimentation. Chemicals for the study were used as received without further purification or modification. For the synthesis and analytical experiments, standard glasswares (Borosil®, Mumbai, India) were used. All other reagents used were of analytical grade. Standard tissue culture plates and cell strainers from HIMEDIA were used in determining biological activities. All glassware were cleaned with aqua-regia prior to experimentation.

2.2. Methods

2.2.1. Synthesis of gold nanoparticle (LuAunp)

Facile, ultrasonically driven green synthesis of gold nanoparticle was carried out using phyto-constituent luteolin, performing dual role of reducer as well as stabilizer. Typically, 3 mL aqueous solution of $HAuCl_4{\cdot}3H_2O$ (1 mM) preconditioned at 40 °C, was placed in a bath sonicator set at the frequency of 40 kHz and power 100 W (LMUC 3, Labman, Chennai, India). 1 mL (3 mM) Lu methanolic solution was added to the gold salt under ultrasonication, maintaining the same reaction conditions for 12 min. Progression of the reduction process was evidenced from incessant colour changes initiating from pale yellow to stable purple on reaction completion. The nanoparticles were finally separated by ultracentrifugation (Himac CS 120 GHXL, Hitachi-Koki, Tokyo, Japan) at 11,800 rpm (~24150 g) for 30 min at 4 ± 2 °C. The synthesis procedure was optimized varying reactant molar ratio and sonication time.

2.2.2. Surface modification of LuAunp with EGF

For target specific biological activity, EGF protein was tagged with prepared LuAunps in two steps. Carboxyl groups were introduced to the LuAunps in the first step. In the second step, EGF was conjugated to LuAunp via amide bond formation through EDC/NHS coupling reaction [27]. Briefly, succinic anhydride (0.5 g, 5.0 mM) and TEA (0.5 g, 5.0 mM) were chronologically added to the LuAunp solution under continuous stirring and kept for 24 h to obtain carboxylated LuAunp [28]. In the next step, carboxylated LuAunp was purified and further dispersed in PBS buffer (pH 7.4). EDC and NHS solutions (both 1 mg/mL) were also prepared in PBS. 250 μL of prepared EDC solution was added drop-wise in the carboxylated nanoparticle solution followed by 5 min of stirring and finally 250 μL of NHS was added drop by drop in the same mixture. The whole mixture was stirred for another 4 h. Thereafter, 100 μL of EGF protein (1 mg/mL) solution was added drop-wise with continuous stirring for 2 h and then incubated overnight at 4 °C. Prepared EGF-LuAunps were purified by centrifugation, re-dispersed in HPLC water and was stored at 4 °C until further use.

FITC tagged EGF-LuAunp was obtained according to the procedure followed by Lin et al. [29]. Briefly, 4 μL of 1 mM FITC solution was added to freshly prepared 4 mL of EGF-LuAunp solution under stirring condition and kept for 45 min in dark condition. After overnight

incubation at 4 °C, FITC tagged EGF-LuAunps were purified by ultra-centrifugation at 11800 r.c.f for 30 min at 4 °C and was stored in refrigerator with protection from light until further use.

2.2.3. Characterization of nanoparticles

The change in the colour of reaction medium from pale yellow to stable purple during the bio-reduction of gold ions was monitored by periodic sampling and subsequent analysis using double beam UV–Vis Spectrophotometer (UV-1900, Shimadzu, Kyoto, Japan). UV–Vis spectra of the samples were monitored applying different sonication time as well as molar ratio. Hydrodynamic diameter, polydispersity index (PDI) and Zeta potentials (ζ) of LuAunps and EGF-LuAunps were analyzed by Zetasizer Nano ZS (Malvern Instruments, Malvern, UK). Fourier Transform Infrared (FTIR) Spectroscopy analysis of LuAunp and EGF-LuAunp were performed in L1280127 Spectrum 3 FT-IR Spectrometer (Parkin Elmer, Massachusetts, United States) to confirm the association of Lu and EGF with the nanoparticles. Dried samples of Lu, LuAunps and EGF-LuAunps were scanned in FTIR over the range of 4000–400 cm^{-1} with a resolution of 2 cm^{-1}. The data obtained was stacked in Perkin Elmer Spectrum™ 10 and ORIGINPRO® software for comparative analysis. Gold sol molar concentration in optimized LuAunp was determined using high resolution inductively coupled plasma mass spectrometry (HR-ICPMS) (Element XR™, Thermo Fisher Scientific, Bremen, Germany) with a concentric nebulizer for normal acid based solution and flow rate of 50–100 μL/min. Synthesized LuAunp was initially digested in aqua regia for 2 h and was diluted in HPLC graded water maintaining a concentration <1 ppm. Gold metal concentration in LuAunp was determined using Au^{197} isotope and the instrument operating conditions maintained were 27 MHz with 2 KW radio frequency power aided by computer controlled three Argon mass flow controller for plasma torch and nebulizer.

Morphological features of synthesized LuAunps and EGF-LuAunps were analyzed in high resolution transmission electron microscope (HRTEM) (JEOL-JEM 2100 HR WITH EELS, Tokyo, Japan). Samples were drop-coated onto carbon-coated copper TEM grids (300 mesh, Ted pella, Redding, CA, USA) and were exposed to TEM analysis in bright field mode at an accelerated voltage of 200 kV. To detect the elemental composition of the optimized nanoparticles, energy dispersive X-ray (EDX) analysis was performed. X-ray diffraction (XRD) analysis was performed on D8 Advance (Bruker, Karlsruhe, Germany) diffractometer at an accelerating voltage of 40 kV. Cu source X-ray was used as the radiation source (wavelength $\lambda = 1.54$ Å) with a current intensity of 40 mA. The applied scanning rate was 0.02°/s in the 2θ range of 20–80°.

2.3. Biological evaluations

2.3.1. Cell culture

MDA-MB-231 and NIH/3T3 cells were cultured in DMEM, supplemented with 10% FBS and 1% antibiotic-antimycotic mix. The cells were maintained in 5% CO_2 atmosphere with 95% humidified air at 37 °C temperature. Growth medium was changed on every alternate day. Trypsin solution (0.05% trypsin-0.02% EDTA) was used to detach the confluent cultures. Cells in the log phase were sub-cultured for further study.

2.3.2. Cellular toxicity study

MDA-MB-231 and NIH/3T3 cells were plated in 96-well plates with cell density of 5×10^3 cells/well and incubated overnight for cell adhesion. Lu (dissolved in DMSO) or LuAunp and EGF-LuAunp (dispersed in HPLC grade-water) were added to appropriate wells in triplicates at varying concentrations (0.5, 1, 2, 4, 8, 12, 16 and 20 μg/mL) and incubated for 24 h. Cells devoid of any added test agents served as the control. After 24 h nanoparticle exposure, cells were washed with 100 μL of sterile PBS to remove particle residues and prevent interference with MTT reagent. The media was discarded after incubation, and MTT reagent (5 mg/mL in PBS, pH 7.4) was added. Plates were incubated for another 4 h at 37 °C in darkness and finally formazan crystals were dissolved in DMSO (100 μL/well). The absorbance was quantified at 570 nm in a Microplate Absorbance Reader. Cell viability was recorded as the ratio of mean absorbance from triplicate findings and calculated as ($A_{test}/A_{control}$) [30].

2.3.3. Cell cycle analysis

MDA-MB-231 cells were plated in 6-well culture plates (density of 1×10^4 cells/well) and treated with Lu, or conjugated nanoparticles, for 24 h. Following incubation, the cells were washed with ice-cold PBS (pH 7.4), re-suspended in PBS and were fixed using 70% ethanol maintained at 4 °C for 15 min. The fixed cells were washed, resuspended and incubated with RNase (100 μg/mL) at 37 °C. The cell pellets were then stained with PI staining solution (50 μg/mL PI, 0.1% sodium citrate, 0.05% Triton X-100) and incubated in dark for 15 min. The DNA content was determined exploring flow cytometer (FACS Aria III; BD Biosciences, USA) and analyzed with BD FACS Diva software [31].

2.3.4. Apoptosis detection assay

MDA-MB-231 cells were harvested after exposure with Lu, LuAunp or EGF-LuAunp for 24 h and re-suspended in Annexin binding buffer. Treated cells were exposed to Annexin V-FITC and PI solution for 10 min in dark environment at 37 °C and fluorescence was recorded. The percentages of apoptotic and necrotic cells were tracked with BD FACS Diva software [31].

2.3.5. Cellular uptake of FITC-tagged nanoparticles

TNBC cells were grown on glass cover slips, introduced in 6-well plates and then treated with FITC-conjugated nanoparticles (FITC-LuAunps and FITC-EGF-LuAunps). After each specified time points (1 h, 2 h and 4 h), cover slips were washed in PBS and the cells were fixed in 4% paraformaldehyde for 15 min at room temperature. Cover slips were co-stained with DAPI and mounted on slides for visualization with FV 1200 Olympus confocal laser scanning microscope followed by image analysis in FV10-ASW 4.1 Viewer [32].

2.3.6. Statistical analysis

Experimental results were analyzed by GraphPad Prism 5.0 (GraphPad Software Inc., USA) and expressed as mean values ± standard deviation (SD) from at least three independent experimental sets. Student's *t*-test was performed for evaluating the comparison between groups. The statistical significance was denoted by *p-value <0.05, **p-value <0.01 and ***p-value <0.001 vs control group; $^{\#}$p-value <0.05, $^{\#\#}$p-value <0.01 and $^{\#\#\#}$p-value <0.001 vs Lu-treated group.

3. Results and discussion

3.1. Synthesis of gold nanoparticle

Current method reports in-situ synthesis of nano-gold using Lu under ultrasonic conditions. Sonochemical synthesis initiate the propagation of pressure wave through the liquid leads to formation, growth and collapse of micrometrical bubbles. The quasi-adiabatic condition during collapse generates extreme heat and pressure within nanoseconds which accelerate the Lu mediated bioreduction of gold sol [33]. The sonic energy further induces brownian motion of the gold particles imparting significant stability. Lu is a secondary metabolite of flavone derivatives and exists as a yellowish dye, naturally obtained from plant *Reseda luteola* L. [34]. The dye is reported to possess anti-inflammatory, anti-oxidant, anti-microbial, anti-cancer activities and neuroprotective actions [35–38].

Primary radicals like hydrogen and hydroxyl radicals generate through sonication induced imploding of water vapor [39]. Lu absorbed at the bubble-solution interface prevents the combination of these primary radicals through radical scavenging effect. The secondary radical with longer life produced thereafter can diffuse in the bulk solution and

propagate further reaction. Completion of reaction was marked by the transient change of colour from pale yellow to deep purple and appearance of steady SPR peak at 541 nm. Gold nanoparticle formation following Frens method [40] of fast nucleation and diffusion-controlled growth was further established by varying the molar ratio of Lu with fixed gold precursor (1:0.4, 1:0.5, 1:0.6, 1:0.7, 1:0.8, 1:0.9, 1:1, 1:1.1). Increasing the molar concentration of Lu up to 3 mM resulted in the maximum intensity of UV-peak with λ_{max} of 541 nm at molar proportion of $HAuCl_4$ to Lu 1:1. At lower concentration of Lu, though fast reduction reaction initiates but aggregation of the primary particles results in polydisperse nanocluster. The aggregation occurs via Van Der Waals interaction as reduced quantity of Lu is present in the reaction medium to coat Au and to stabilize the particles [41]. After some time, aggregation stops and nanoparticle growth occurs via diffusion method which leads to the formation of larger particles at lower molar ratio (Table 1). Increase in Lu concentration results in complete reduction reaction which is evident from the increase in the intensity of the SPR peak at 541 nm. When the concentration of Lu increases, it adequately envelops nanoparticle surface and prevents agglomeration by electrostatic repulsion between the particles which can be linked to traditional nucleation and growth model giving rise to spherical Aunps [42]. When the critical condition was achieved, a significant bathochromic shift with less peak intensity was observed in UV response for further increase in Lu concentration which may be linked to the particle aggregation and irregular LuAunp formation in the reaction environment (Fig. 1A).

Gold reduction reaction initiates after 6 min of reaction as evidenced by the occurrence of colour change and also by SPR recorded in UV–Vis spectroscopy. To optimize the reaction time for LuAunp synthesis, different sonication time (6 min, 7 min, 8 min, 9 min, 10 min, 11 min, 12 min, 13 min) was also experimented. Mild preheating of reaction solution to 40 °C was instrumental for efficient formation of reducing radical which promote the reduction. At shorter sonication time (6 min) SPR peak corresponding to LuAunp was observed at longer wavelength with less intensity (Table 2).

The reduction process rapidly occurred due to irradiation but if irradiation stops, random attachment process predominates over nucleation which results in heterogeneous particles of larger size. Gold precursor $HAuCl_4$ first undergoes hydrolysis to form Au^{3+} which after induction of sonic energy participates in the redox reaction. During reduction Lu gets oxidised and the electrons released from it assists the reduction process of Au^{3+} to intermediate complex. Longer sonication time creates suitable condition to generate higher concentration of this complex which gets transformed into Au^0 [43]. The highest plasmonic peak intensity was observed at 541 nm after 12 min of sonication (Fig. 1B). After reaching the critical time point, where all the redox reactions continuously occurring in the media achieves equilibrium, a further increase in sonication time, shifting of SPR peak to 553 nm from 541 nm was observed with decreased intensity which might be related to high velocity collision among the particles resulting in particle-particle fusion [44].

Lu mediated reduction of Au^{+3} to Au^0 was not possible without sonication as no colour change was observed even after 2 h of observation period. At lower temperature, the reduction potential of Lu alone was not sufficient enough to initiate Au nuclear transformations [21]. Interestingly, when the solution mixture of $HAuCl_4$ and Lu in the optimized molar ratio was heated at 80 °C for 10 min without sonication, the SPR peak was observed at 562.5 nm with colour transformation from pale yellow to blue followed by rapid precipitation. In absence of sonication slow reduction occurred with adsorption of gold (III) chloride on the nanoparticle surface resulting in weak flocculation. Blend of sonication and heating accelerated the replacement of gold (III) chloride on nanoparticle surface by Lu leading to enhancement of surface charge and peptization of the sol imparting nanoparticle stability [41]. Stability of the nanoparticles was monitored via UV-VIS spectroscopy at different intervals of 3, 7, 15 and 30 days. The maximum absorption of incident light remains around λ_{max} of 541 nm indicating minimal changes of nanoparticle dimension with limited agglomeration.

Lu is a polyphenolic compound with four hydroxyl (OH) groups in its structure. The reaction mechanism for LuAunp synthesis proceeds via reduction of Au^{3+} to Au^0 where Lu plays the dual role of reducing and stabilizing agent. Lu initiates the reduction process by quick abstractions of the most labile H-atoms from 3′-OH and 4′-OH group (Fig. 2) [21]. As a result, Lu might itself gets oxidised by converting 3′,4′-dihydroxy phenyl moiety to ortho-quinone via free radical mechanism. The free radical intermediate gets stabilized due to the resonance of chromene ring system, probably through the carbonyl group present at 4th position of Lu [45]. Lu also provides the stability of Aunp's by interacting with nanoparticle facets which ensures the blocking of further interactions between nanoparticles and restricts agglomeration. In the next step, free OH group present in LuAunp was carboxylated with succinic anhydride [28] and then EGF was conjugated to modified LuAunp through carbodiimide chemistry as described in Fig. 2.

Table 1
Effect of change in molar ratio of reactants on particle characteristics.

Molar ratio (Gold precursor: Lu)	SPR (nm)	Hydrodynamic diameter (nm)	PDI	Zeta potential (mV)
1:0.4	601	95.4 ± 7.06	0.312 ± 0.01	−8.55 ± 1.46
1:0.5	589	86.89 ± 6.22	0.297 ± 0.02	−9.7 ± 2.01
1:0.6	538.5	56.32 ± 3.36	0.244 ± 0.02	−16.67 ± 2.23
1:0.7	536	53.97 ± 5.77	0.219 ± 0.01	−17.78 ± 1.4
1:0.8	540	61.05 ± 4.5	0.253 ± 0.01	−18.1 ± 2.55
1:0.9	539	58.85 ± 5.06	0.260 ± 0.01	−20.84 ± 1.09
1:1	541*	65.12 ± 4.54	0.257 ± 0.01	−24 ± 1.73
1:1.1	532	51.29 ± 8.97	0.225 ± 0.01	−17.2 ± 2.89

Results expressed as mean ± Standard Deviation (n = 3). *Highest absorbance was recorded for SPR (λ max) 541 nm with molar ratio of 1 : 1 [Gold precursor: Lu].

3.2. Characterization of nanoparticles (LuAunps and EGF-LuAunps)

3.2.1. Particle size and zeta potential

To determine particle size, size distribution, polydispersity index (PDI) and zeta potential of LuAunp and EGF-LuAunp, dynamic light scattering (DLS) method was used. Extensive and repeated experimentation were carried out to develop a suitable and optimized route to achieve better particle attributes. Variation in particle characteristics with change in molar ratio or sonication time is tabulated in Tables 1 and 2.

Therefore optimized formulation with 1:1 M ratio of Lu:Gold precursor and 12 min of sonication time was used for further studies.

DLS or photon correlation spectroscopy (PCS), is a sophisticated analytical technique interprets the diffusion coefficient, and hence the hydrodynamic mean diameter *d(H)* using Stokes-Einstein equation [46]. The particle distribution data of LuAunp suggests a gaussian-shaped distribution (Refer Supplementary Data) with moderate polydispersity index.

Zeta potential on the other hand gives an insight on net surface charge of any dispersed particle in a colloidal solution and its stability [47]. The high zeta potential of both nanoparticles with a characteristic V-shaped phase plot indicates that they are negatively charged and highly stable particles. In line with our earlier report, protein tagged nanoparticles exhibited a significant enhancement of net negative charge due to the protein linkage [48].

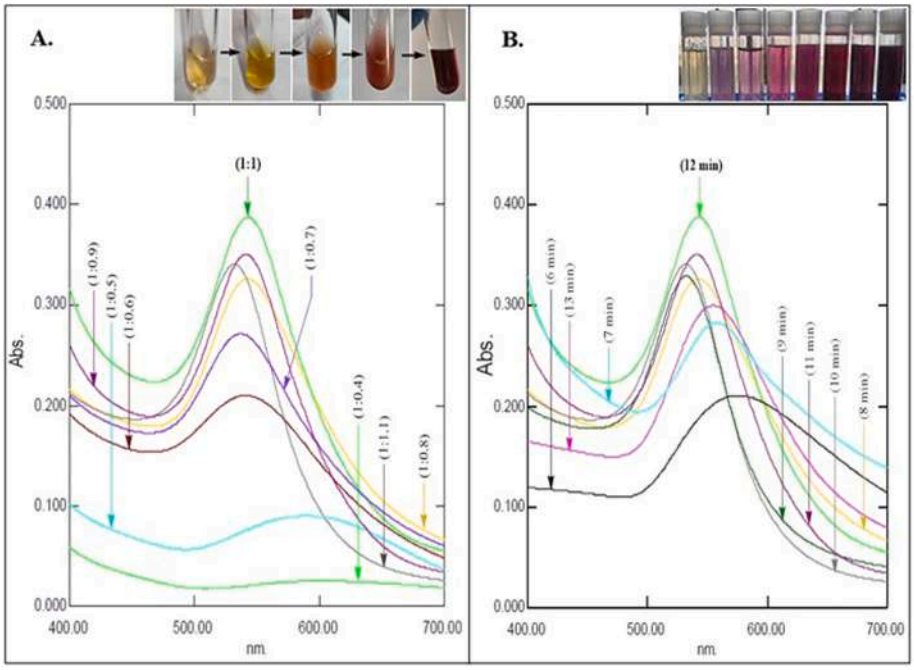

Fig. 1. Characterization of nanoparticles using UV–Vis spectroscopy. (A) UV–Vis spectra of LuAunp with varying molar proportion of gold chloride and Lu i.e. from 1:0.4 to 1:1.1; Inset Fig. 1A: Colour variations during molar ratio optimization. Transformation from deep yellow to stable purple confirms reaction completion. (B) UV–Vis spectra obtained varying reaction time points i.e. from 6 min, to 13 min; Inset Fig. 1B: Colour variations during molar ratio optimization. (For interpretation of the references to colour in this figure legend, the reader is referred to the Web version of this article.)

Table 2
Effect of change in sonication time on particle characteristics.

Time point (min)	SPR (nm)	Hydrodynamic diameter (nm)	PDI	Zeta potential (mV)
6	572	80.46 ± 6.6	0.290 ± 0.02	−10.2 ± 3.1
7	557	70.15 ± 4.22	0.277 ± 0.01	−14.37 ± 2.8
8	544	69.1 ± 3.77	0.271 ± 0.01	−14.89 ± 2.1
9	532	51.97 ± 5.77	0.233 ± 0.02	−17.64 ± 2.8
10	530	50.08 ± 4.97	0.269 ± 0.01	−18 ± 2.33
11	540	62.3 ± 4.55	0.264 ± 0.02	−23.5 ± 1.65
12	541*	65.12 ± 4.54	0.257 ± 0.01	−24.0 ± 1.73
13	554	69.23 ± 7.97	0.271 ± 0.01	−15.06 ± 2.4

Results expressed as mean ± Standard Deviation (n = 3). *Highest absorbance was recorded for SPR (λ_{max}) 541 nm with 12 min sonication time.

3.2.2. TEM analysis

HRTEM analysis is a powerful tool that allows studying of the properties of materials on the atomic scale. HRTEM images of typical LuAunp and EGF-LuAunp populations were shown in Fig. 3A and B. LuAunp HRTEM analysis suggested that the particles having nearly spherical geometry without noticeable aggregates with an average diameter of 25.12 nm. Few triangular and hexagonal plates with side length of 38.72 nm was also found. Chloride ion produced during reduction of $AuCl^{4-}$ contributes in the growth of crystals resulting in different particle shapes. Adsorption of chloride ion on specific crystal facets promotes the formation of triangular and/or hexagonal plates present in our zone of observation [49]. The size distribution histogram was developed with 100 particle counts. The average particle diameter (D) 25.12 nm for LuAunp and 30.23 nm for EGF-LuAunp with standard deviations (σ) 10.35 and 9.96 for LuAunp and EGF-LuAunp (Fig. 3C and D) respectively [45]. Both nanoparticle population in HRTEM exhibits fairly mono-dispersed particles with few of higher size range as reflected in size distribution histogram.

Single LuAunp and its selected area electron diffraction pattern (SAED) in HRTEM are illustrated in Fig. 3E and F. HRTEM observation of EGF-LuAunp suggested that nano-gold formulation is having crystal growth lattice planes with lattice fringe spacing of 0.173 nm [50]. The clear lattice fringes were observed in HRTEM image and the bright circular rings correspond to (1 1 1), (2 0 0), (2 2 0) and (3 1 1) planes were recorded.

3.2.3. EDX, HR-ICPMS and XRD analysis

EDX was performed to investigate about the elemental composition of LuAunps. The EDX spectrum indicated the presence of gold (Au) with oxygen (O) and carbon (C) atom. The presence of 'O' and 'C' suggests the association of Lu with gold atoms. However, a small chlorine (Cl) peak was present which may have formed during the reduction process (Fig. 4A). HR-ICPMS analysis of gold (Au) concentration in LuAunp dispersed in aqueous medium confirmed Au^0 concentration at 156 μg/mL Au. XRD spectra of LuAunp is illustrated in Fig. 4B. Bragg's diffraction peaks of purified LuAunp was indexed for (1 1 1), (2 0 0), (2 2 0), (3 1 1) sets of lattice plane at 38.00°, 44.62°, 64.72° and 77.68° respectively, reflecting the formation of face centric cubic (fcc) structure of metallic gold. It is also noticeable that the formation of nano-gold crystals was mainly induced by (1 1 1) facets of metallic gold as it was recorded having a sharp signal as compared to other lattice planes [51].

3.2.4. FTIR spectroscopy

FTIR spectra helps to identify organic compounds by determining different functional groups depending on the vibrational properties of molecules when get excited at specific wavelength after exposure to IR radiation [52]. The FT-IR spectra of Lu, LuAunp and EGF-LuAunp were recorded and overlayed altogether taking wavenumber (cm^{-1}) in x-axis and transmittance (a.u.) in the y-axis (Fig. 4C) to detect Lu and EGF interaction with gold nanoparticles. Lu showed the characteristic peaks at 3423, 1612, 1503, 1170 cm^{-1} for phenolic –OH, ketone (C═O), aromatic unsaturation hydrocarbon (C═C) stretching, and etheric linkage (C–*O*–C) [53]. The FTIR spectra of LuAunp showed broad peak at 3160 cm^{-1} possibly due to the interaction between the nanoparticle and the phenolic –OH group of Lu. The characteristic peaks for C═O, aromatic C═C and C–*O*–C stretching were well observed at 1612, 1502, and 1165 cm^{-1} which confirm the conjugation of Lu as well as the stability of the

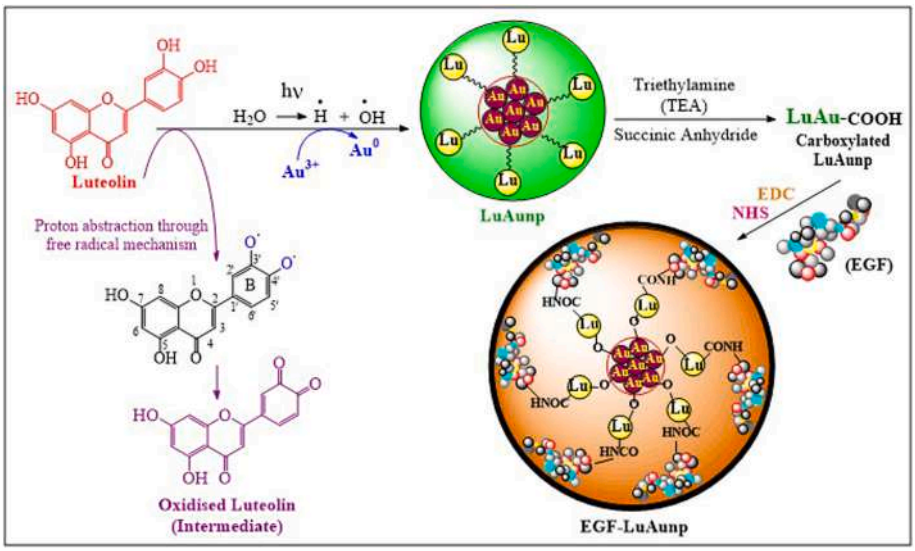

Fig. 2. Plausible reaction route for EGF-LuAunp synthesis.

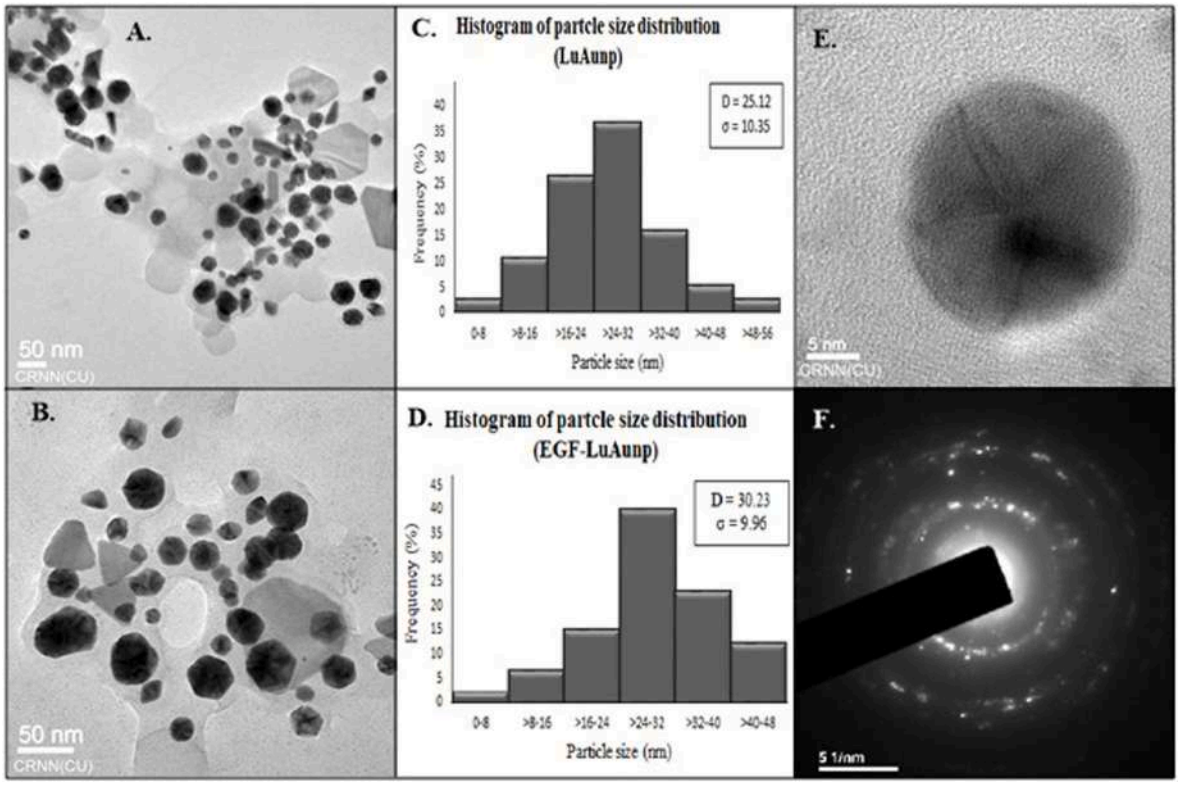

Fig. 3. Nanoparticle characterizations. (A) HRTEM micrograph of nanoparticle (LuAunp) population. (B) HRTEM micrograph of nanoparticle (EGF-LuAunp) population. (C) Histogram of nanoparticle (LuAunp) size distribution. (D) Histogram of nanoparticle (EGF-LuAunp) size distribution (E) High resolution TEM micrograph of single EGF-LuAunp. (F) SAED pattern for EGF-LuAunp.

aromaticity of Lu in nanoparticles [51,54].

In case of EGF-LuAunp, the peaks at 1610 and 1086 cm^{-1} could be assigned for the C═O and C–*O*–C linkage suggesting the suitable special orientation of ketone and ether. A shift in the hydroxyl absorption band was well observed which merges with the peak for amine (-NH_2) at 3401 cm^{-1} which could be attributed to the change in the capability of hydrogen bond after the attachment of EGF. The characteristic amide carbonyl (-CONH) peak was recorded at 1653 cm^{-1} in EGF-LuAunp that could be linked to the α-helical coil structure arrangement of the protein. These peaks findings indicate the conjugation of the protein to nanoparticles [55,56].

3.3. Biological evaluations

3.3.1. Cytotoxicity of Lu, LuAunps and EGF-LuAunps

The anti-proliferative and cytotoxic effects of Lu, LuAunp and EGF-LuAunp were evaluated using MTT assay of treated as well as untreated cells. Dose-dependent studies were performed considering the gold concentration of respective formulations to calculate IC_{50} value. Cell viabilities of MDA-MB-231 cells was recorded after exposure to

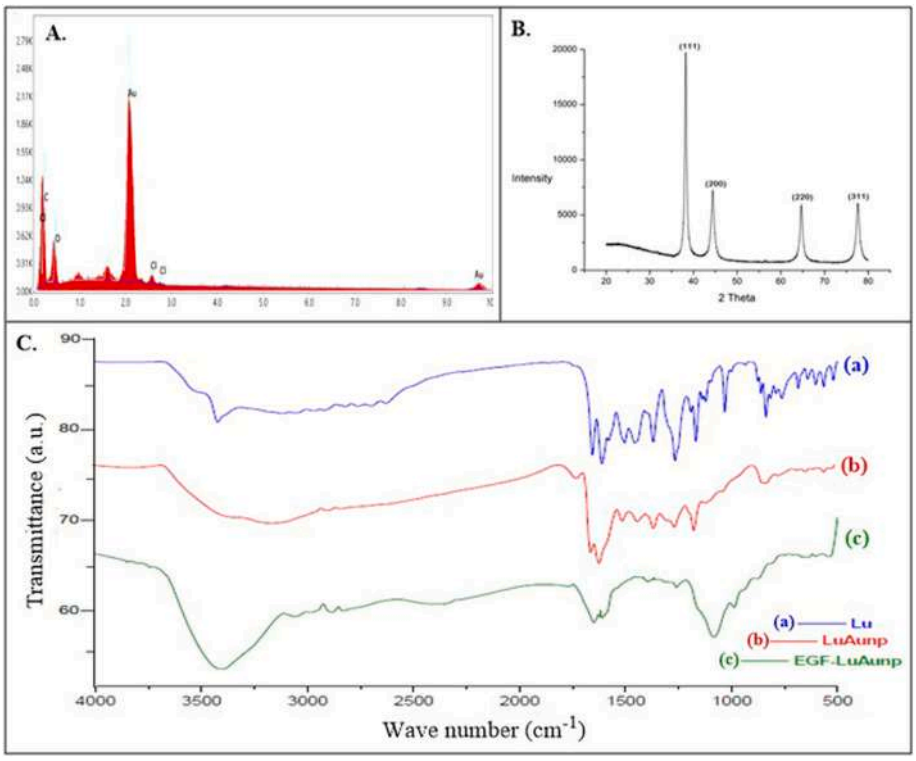

Fig. 4. Nanoparticle characterization. (A) EDX pattern of EGF-LuAunp. (B) XRD spectra of EGF-LuAunp. (C) FTIR spectra of (a) Lu (b) LuAunp (c) EGF-LuAunp.

varying concentrations (0.5–20 μg/mL) of Lu. Subsequently, effects of LuAunp and EGF-LuAunp were analyzed using equivalent concentrations of Lu. Results indicated a significant decrease in viability of the TNBC cells. The IC_{50} of Lu was assessed to be 12 μg/mL, whereas that for LuAunp was 4 μg/mL and for EGF-LuAunp was 2 μg/mL (Fig. 5A). In case of NIH/3T3 cells, neither Lu nor the conjugated nanoparticles showed any significant inhibitory effects on cell viability, compared to the untreated cells, suggesting that Lu, LuAunp and EGF-LuAunp, at concentrations up to 12 μg/mL, are not toxic for the normal cells (Fig. 5B).

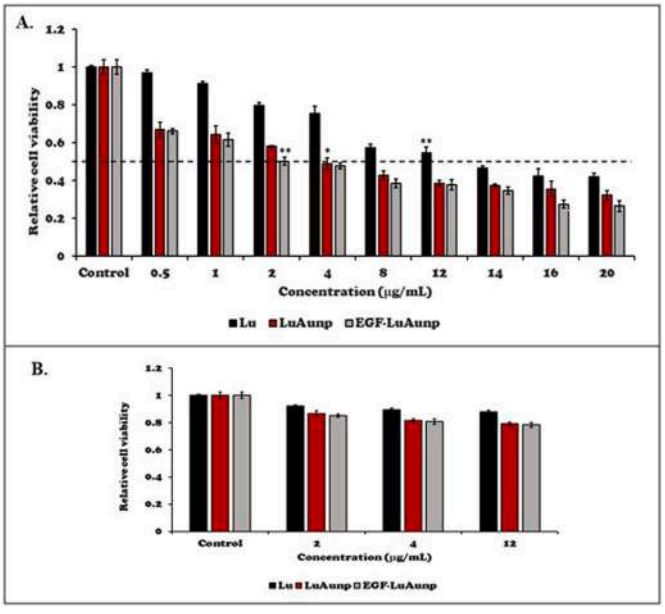

Fig. 5. Cellular cytotoxicity analysis. MTT assay of Lu, LuAunp and EGF-LuAunp on (A) MDA-MB-231 cells (B) NIH/3T3 cells. Neither the free drug nor the conjugated nanoparticles demonstrated cytotoxicity on the transformed fibroblast cells, whereas the effect on the TNBC cells was radical.*$p < 0.05$ and **$p < 0.01$ vs. control group.

Therapeutic targeting is a major clinical challenge in TNBC because of the lack of ER, PR and HER2 expression. However, a significant number of TNBC cases exhibits elevated EGFR expression [57,58], and therefore EGFR targeted therapies are becoming attractive alternatives in treating this cancer variant [59]. In the present study, EGF was thus selected as a targeting ligand for tethering on gold nanoparticles to induce enhanced anti-cancer efficacy through site-directed approach. Cellular toxicity evaluations by MTT analysis suggested that high concentrations of Lu (12 μg/mL) exhibited anti-proliferative effect on MDA-MB-231 cells. This was in accordance with a study performed by Liming et al. (2019), who demonstrated a dose-dependent anti-tumor effect of Lu on MDA-MB-231 cells [60]. Interestingly, EGF-LuAunps showed significantly pronounced anti-proliferative and cytotoxic effects on MDA-MB-231 cells at a lower IC_{50} value as compared to both LuAunps (by 6-fold) and free Lu (by 3-fold). Improvement in the cytotoxic effects at lower concentrations of EGF-LuAunps might have stemmed from EGF-mediated specific cellular uptake. On the contrary, NIH/3T3 mouse fibroblast cells were not significantly affected by the Lu, LuAunps and EGF-LuAunps, suggesting that the conjugated nanoparticles are specifically toxic to cancer cells favouring further clinical explorations. Lu cyto-compatibility towards NIH/3T3 cells was in line with pre-clinical reports by other researchers [61].

3.3.2. *Effects of Lu, LuAunps and EGF-LuAunps on cell cycle*

The influence of Lu, LuAunps and EGF-LuAunps on proliferation of TNBC cells were analyzed using flow cytometry. The study investigated whether cell cycle intervention directed growth suppression, induced by the test samples. Cell cycle phase distribution of MDA-MB-231 cells was monitored after treating with IC_{50} concentrations of the free and conjugated compounds for 24 h. The fraction of cells in different phases of the cell cycle were assessed and recorded (Fig. 6A). MDA-MB-231 cells exhibited a sharp decline in G_2/M phase, as compared with control, following Lu treatment, along with a rise in cell population in the sub-G_1

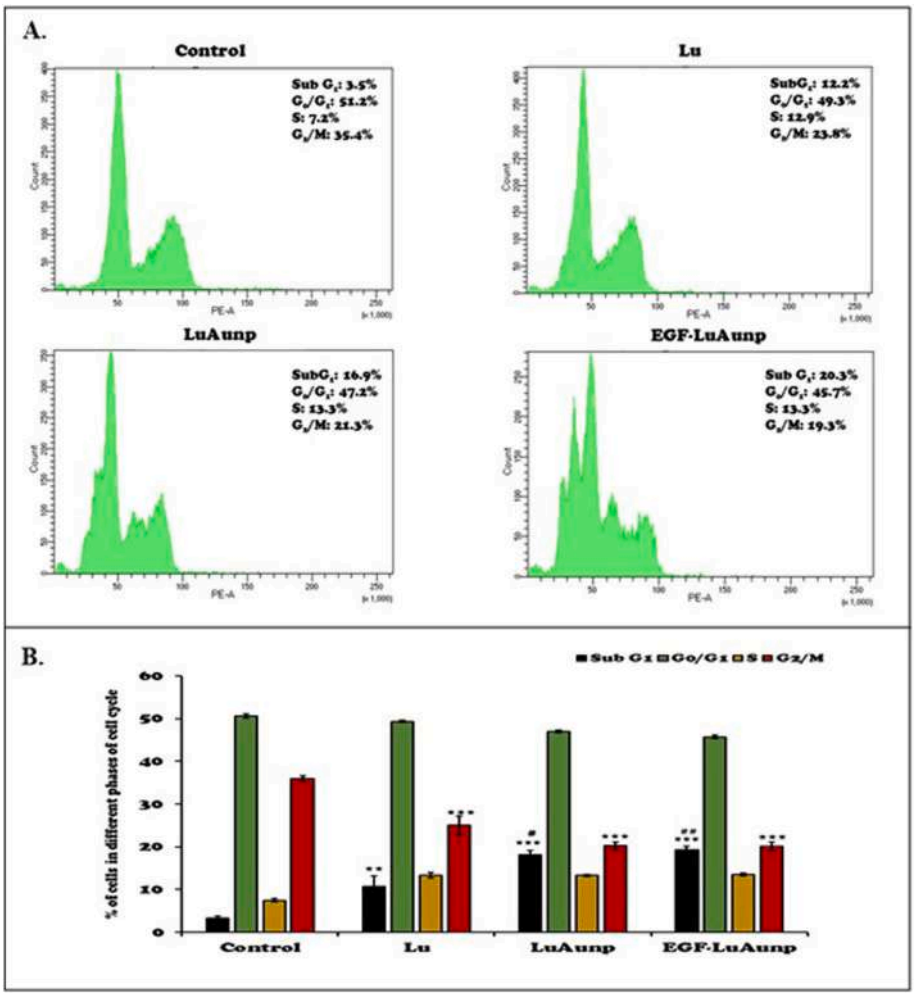

Fig. 6. Lu, LuAunps and EGF-LuAunps lead to an escalation in the sub-G_1 population. (A) Cell cycle analysis of free Lu, LuAunp and EGF-LuAunp on TNBC MDA-MB-231 cell line with respect to control (untreated) cells. (B) Quantitative analysis of cell cycle phase distribution. $^{**}p < 0.01$ and $^{***}p < 0.001$ vs. the control group and $^{\#}p < 0.05$, $^{\#\#}p < 0.01$ vs. Lu-treated cells.

phase. The cellular fraction in sub-G_1 phase for the control group was 3.5% while that for Lu was 12.2%, LuAunp was 16.9% and EGF-LuAunp was 20.3% (Fig. 6A). Quantitative analysis of the same has been demonstrated in Fig. 6B.

Consistent with previous report [60], cell cycle analysis by flow cytometry revealed an enhancement in the sub-G_1 cellular population with concomitant reduction in G_2/M phase, most significantly by EGF-LuAunp, followed by LuAunp and least by the free Lu. A considerable accumulation of cells at sub-G1 phases may be likely due to down-regulation of cell cycle regulatory genes important for G1 phase transition [62].

3.3.3. *Effects of Lu, LuAunps and EGF-LuAunps on cell death*

As Lu and conjugated nanoparticles inhibited progression of breast cancer cells *in vitro*, their pro-apoptotic effects on MDA-MB-231 cells were examined using Annexin V-PI assay by flow cytometry. As shown in Fig. 7A, there is a significant upsurge in the incidence of cell death with consequent reduction in live cell population following treatment with Lu, LuAunp and EGF-LuAunp when equated with DMSO-treated control group. After 24 h exposure, there is apoptotic, as well as necrotic, cell death following treatment. Quantitative data revealed that the reduction in the percentage of live cells was achieved more significantly (p-value <0.01) by EGF-LuAunp than LuAunp's (p-value <0.05) with respect to free Lu. This contributed to the enhanced efficiency of EGF-LuAunp in inducing cell death in TNBC cells than the latter test agents (Fig. 7B).

Therefore, Annexin V-PI assay by flow cytometry ascertained that LuAunp influenced significant death of TNBC cells. Increased population of sub-G_1 cells along with a greater percentage of dead cell population in EGF-LuAunp's treated group strengthen the fact that they can be a fascinating proposition as competent targeted therapeutics for TNBC management.

3.3.4. *Cellular uptake of FITC tagged LuAunps and EGF-LuAunps*

Cellular uptake studies were performed using FITC-labelled nanoparticles LuAunps and EGF-LuAunps. Confocal microscopy images in MDA-MB-231 cells were recorded after being exposed to FITC-labelled nanoparticles for 1 h, 2 h and 4 h. Time-dependent increase in FITC green fluorescence was observed due to cytoplasmic accumulation of nanoparticles in MDA-MB-231 cells. Cellular uptake of EGF-LuAunp in MDA-MB-231 cells was quite perceivable within 1 h of incubation, suggesting an efficient uptake. However, in case of LuAunp, speedy internalization was not observed which might be responsible for its reduced efficacy as compared to EGF-LuAunps against cancer cells (Fig. 8A and B).

Enhanced cellular uptake coupled with apoptosis of TNBC cells thus confer EGF-LuAunps to be an ideal candidate as anti-cancer therapeutics.

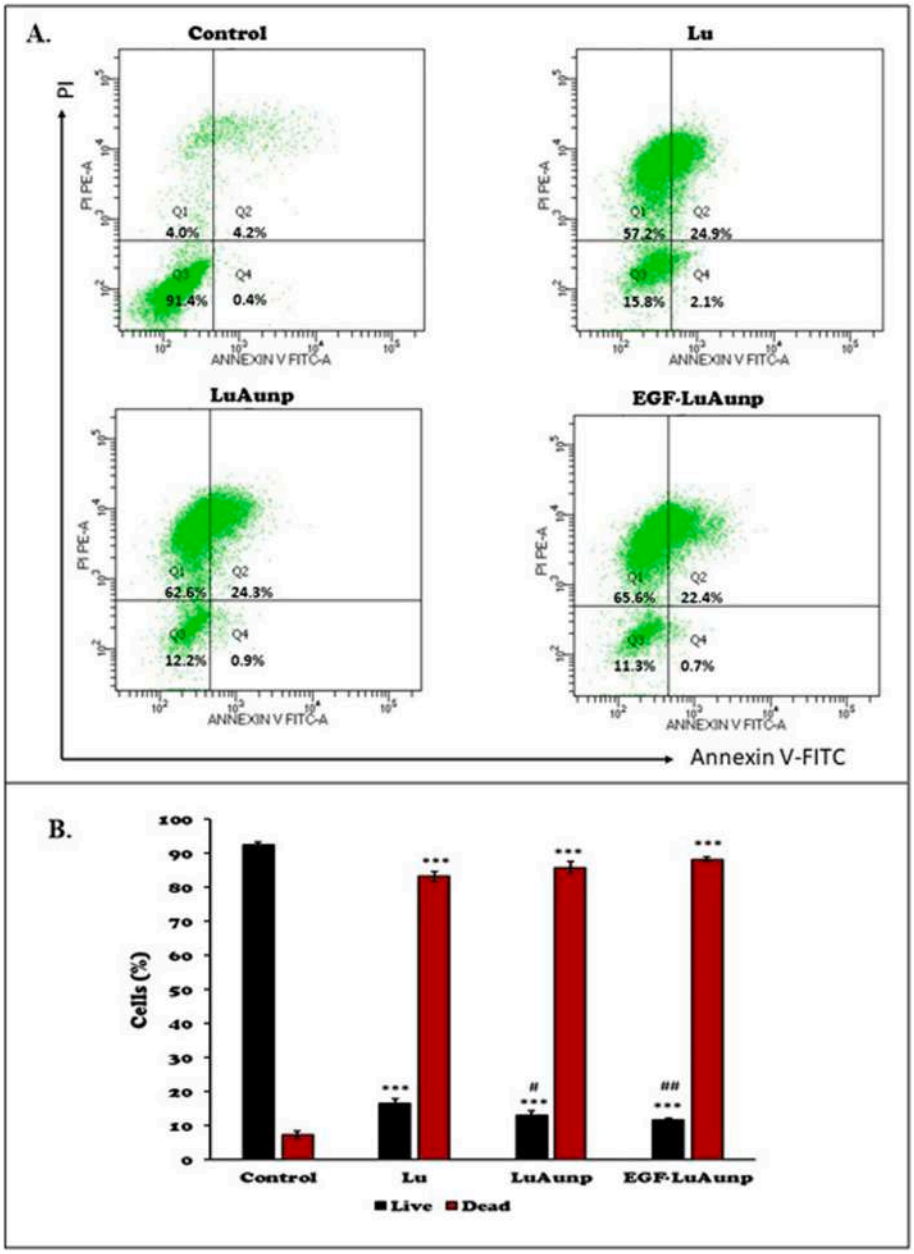

Fig. 7. Effect of Lu and the nanoparticle conjugates on the cell death. (A) Representative flow cytometry plots examining cell death in TNBC MDA-MB-231 cell line following free Lu, LuAunp and EGF-LuAunp treatment using Annexin V-PI staining. $FITC^{-ve}/PI^{-ve}$ (Q3) cells were designated as "live cells", $FITC^{+ve}/PI^{-ve}$ (Q4) as "early apoptotic cells", $FITC^{+ve}/PI^{+ve}$ (Q2) as "late apoptotic cells" and $FITC^{-ve}/PI^{+ve}$ (Q1) as "necrotic cells". (B) Quantitative analysis of cell death determined using Annexin-V/PI assay. The dead cell population included the early apoptotic cells (Q4), late apoptotic cells (Q2) and necrotic cells (Q1). ***$p < 0.001$ vs. control group and $^{\#}p < 0.05$, $^{\#\#}p < 0.01$ vs. Lu group.

4. Conclusion

Flavonoid conjugated synthesis of gold nanoparticles was achieved by means of a facile and speedy technique with avoidance of hazardous chemicals. Gold nanoparticles majorly of spherical geometry with a diameter around 30 nm were confirmed through HRTEM. The stable nanoparticles were crystalline in nature in which EGF protein was tagged for intended site-specificity to EGFR of TNBC cells. Targeted nanoparticles synthesized exhibited remarkable cytotoxicity against triple negative breast cancer cells which far better than the free flavonoid and non-targeted nanoparticles. Apoptosis assay and cell cycle analysis confirmed significant reduction in cell viability at G2/M phase. Additionally, EGF tagged nanoparticles synthesized also proved its bio-safety by minimal expression of cytotoxicity against non-malignant cells. However, the agglomeration tendency of gold nanoparticles can be a matter of concern as it is influenced by the presence of ions, sugars, pH etc. present in diverse environments like cell culture media and physiological fluids. Therefore, the present work envisages significant potential for further translation into pre-clinical and clinical evaluation stages. Thus, the scientific strategy cements the place of targeted biosafe gold nanoparticles in TNBC management and warrants further *in vitro* & *in vivo* investigations.

CRediT authorship contribution statement

Suvadeep Mal: Methodology, Validation, Investigation, Writing-Original Draft Tiyasa Saha: Methodology, Investigation Asim Halder: Formal Analysis, Validation Sudhir Kumar Paidesetty: Supervision, Formal analysis Suvadra Das: Supervision, Formal Analysis, Validation, Writing-Review & Editing Wong Tin Wui: Supervision, Validation, Writing-Review & Editing Urmi Chatterji: Supervision, Methodology, Validation, Writing-Review & Editing Partha Roy: Conceptualization, Project administration, Writing-Review & Editing, Funding acquisition.

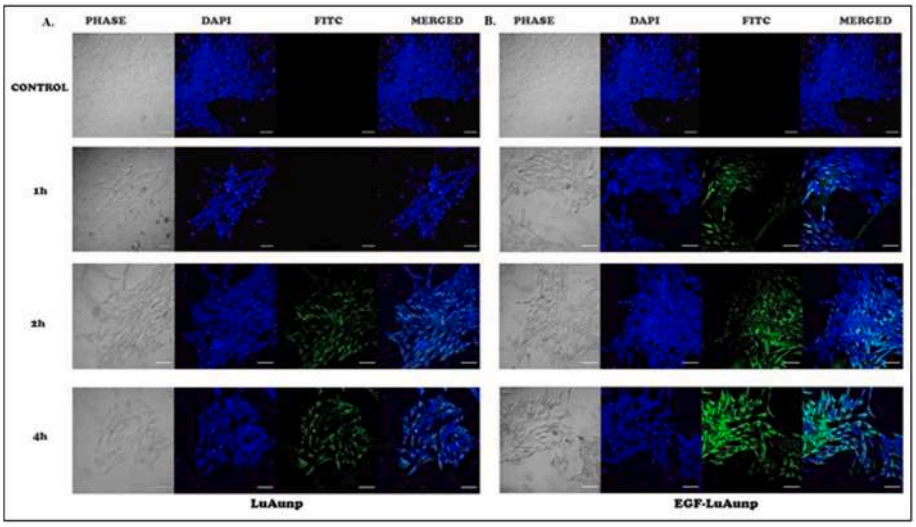

Fig. 8. Cellular uptake and intra-cellular localization of FITC-tagged (A) LuAunps and (B) EGF-LuAunps in MDA-MB-231 cells. MDA-MB-231 cells were exposed to FITC tagged LuAunps and EGF-LuAunps for 1 h, 2 h and 4 h. Each sample was co-stained with DAPI and images were recorded at 40X (scale: 100 μm).

Funding

This work was supported by DST-SERB Asean Grant [IMRC/AISTDF/CRD/20191000133] to Dr. Partha Roy.

Declarations of competing interest

The authors declare no conflict of interest.

Data availability

No data was used for the research described in the article.

Acknowledgement

X-ray powder diffraction (XRD) measurement has been performed at UGC DAE Consortium for Scientific Research, Kolkata Centre. Authors would like to express their gratitude to Dr. P. V. Rajesh for conducting the XRD study, Prof Sriparna Datta from University of Calcutta for DLS studies and SAIF, IIT Bombay for ICPMS study. The authors would like to thank CRNN, University of Calcutta for performing HR-TEM analysis to characterize particle morphology. Relentless supports from Dean SOMS, Adamas University, Chancellor UEM Kolkata and Dean SPS, SOA University (Deemed to be University) throughout the entire work tenure are also heartily acknowledged.

Appendix A. Supplementary data

Supplementary data to this article can be found online at https://doi.org/10.1016/j.jddst.2022.104148.

References

[1] Cancer - WHO, World Health organization. https://www.who.int/Newsroom/Fact sheets/Detail/, 2022. (Accessed 3 February 2022).
[2] E.R. Velazquez, C. Parmar, Y. Liu, T.P. Coroller, G. Cruz, O. Stringfield, Z. Ye, M. Makrigiorgos, F. Fennessy, R.H. Mak, R. Gillies, Somatic mutations drive distinct imaging phenotypes in lung cancer, Can. Res. 77 (2017) 3922–3930, https://doi.org/10.1158/0008-5472.CAN-17-0122.
[3] T. Ovcaricek, S.G. Frkovic, E. Matos, B. Mozina, S. Borstnar, Triple negative breast cancer–prognostic factors and survival, Radiol. Oncol. 45 (2011) 46, https://doi.org/10.2478/v10019-010-0054-4.
[4] A.M. Brewster, M. Chavez-MacGregor, P. Brown, Epidemiology, biology, and treatment of triple-negative breast cancer in women of African ancestry, Lancet Oncol. 15 (2014) e625–e634, https://doi.org/10.1016/S1470-2045(14)70364-X.
[5] E.C. Dietze, C. Sistrunk, G. Miranda-Carboni, R. O'regan, V.L. Seewaldt, Triple-negative breast cancer in African-American women: disparities versus biology, Nat. Rev. Cancer 15 (2015) 248–254, https://doi.org/10.1038/nrc3896.
[6] M.A. Medina, G. Oza, A. Sharma, L.G. Arriaga, J.M. Hernández Hernández, V. M. Rotello, J.T. Ramirez, Triple-negative breast cancer: a review of conventional and advanced therapeutic strategies, Int. J. Environ. Res. Publ. Health 17 (2020) 2078, https://doi.org/10.3390/ijerph17062078.
[7] D. Kashyap, H.S. Tuli, Flavonoids in triple negative breast cancer: chemopreventive phytonutrients, Arch. Can. Res. 6 (2018) 2017–2018, https://doi.org/10.21767/2254-6081.100170.
[8] M. Imran, A. Rauf, T. Abu-Izneid, M. Nadeem, M.A. Shariati, I.A. Khan, A. Imran, I. E. Orhan, M. Rizwan, M. Atif, T.A. Gondal, Luteolin, a flavonoid, as an anticancer agent: a review, Biomed. Pharmacother. 112 (2019), 108612, https://doi.org/10.1016/j.biopha.2019.108612.
[9] Y. Wang, J. Wang, X. Gong, X. Wen, X. Gu, Luteolin: anti-breast cancer effects and mechanisms, J. Explor. Res. Pharmacol. 3 (2018) 85–90.
[10] T.S. Chan, G. Galati, A.S. Pannala, C. Rice-Evans, P.J. O'Brien, Simultaneous detection of the antioxidant and pro-oxidant activity of dietary polyphenolics in a peroxidase system, Free Radic. Res. 37 (2003) 787–794, https://doi.org/10.1080/1071576031000094899.
[11] J. Liu, Y. Sun, M. Cheng, Q. Liu, W. Liu, C. Gao, J. Feng, Y. Jin, L. Tu, Improving oral bioavailability of luteolin nanocrystals by surface modification of sodium dodecyl sulfate, AAPS PharmSciTech 22 (2021) 1, https://doi.org/10.1208/s12249-021-02012-y.
[12] C.A. Hudis, L. Gianni, Triple-negative breast cancer: an unmet medical need, Oncol. 16 (2011) 1, https://doi.org/10.1634/theoncologist.2011-S1-01.
[13] A.G. De Herreros, S. Peiró, M. Nassour, P. Savagner, Snail family regulation and epithelial mesenchymal transitions in breast cancer progression, J. Mammary Gland Biol. Neoplasia 15 (2010) 135–147, https://doi.org/10.1007/s10911-010-9179-8.
[14] F.C. Geyer, M. Lacroix-Triki, K. Savage, M. Arnedos, M.B. Lambros, A. MacKay, R. Natrajan, J.S. Reis-Filho, β-Catenin pathway activation in breast cancer is associated with triple-negative phenotype but not with CTNNB1 mutation, Mod. Pathol. 24 (2011) 209–231, https://doi.org/10.1038/modpathol.2010.205.
[15] D. Lin, G. Kuang, J. Wan, X. Zhang, H. Li, X. Gong, H. Li, Luteolin suppresses the metastasis of triple-negative breast cancer by reversing epithelial-to-mesenchymal transition via downregulation of β-catenin expression, Oncol. Rep. 37 (2017) 895–902, https://doi.org/10.3892/or.2016.5311.
[16] M.T. Cook, Y. Liang, C. Besch-Williford, S.M. Hyder, Luteolin inhibits lung metastasis, cell migration, and viability of triple-negative breast cancer cells, Breast Cancer 9 (2016) 9–19, https://doi.org/10.2147/BCTT.S124860.
[17] E.J. Lee, S.Y. Oh, M.K. Sung, Luteolin exerts anti-tumor activity through the suppression of epidermal growth factor receptor-mediated pathway in MDA-MB-231 ER-negative breast cancer cells, Food Chem. Toxicol. 50 (2012) 4136–4143, https://doi.org/10.1016/j.fct.2012.08.025.
[18] C. Massard, C. Dubois, V. Raspal, P. Daumar, Y. Sibaud, E. Mounetou, M. Bamdad, O. Awitor, Cytotoxicity study of gold nanoparticles on the basal-like triple-negative HCC-1937 breast cancer cell line, J. Biomaterials Nanobiotechnol. 9 (2018) 13–25, https://doi.org/10.4236/jbnb.2018.91002.
[19] S.K. Surapaneni, S. Bashir, K. Tikoo, Gold nanoparticles-induced cytotoxicity in triple negative breast cancer involves different epigenetic alterations depending upon the surface charge, Sci. Rep. 8 (2018), 12295, https://doi.org/10.1038/s41598-018-30541-3.
[20] M.L. Castilho, V.P.S. Jesus, P.F.A. Vieira, K.C. Hewitt, L. Raniero, Chlorin e6-EGF conjugated gold nanoparticles as a nanomedicine based therapeutic agent for triple

negative breast cancer, Photodiagnosis Photodyn. Ther. 33 (2021), 102186, https://doi.org/10.1016/j.pdpdt.2021.102186.
[21] A.H. Yang, X.Y. Shi, X. Li, F.F. Li, Q.Q. Zhang, S.X. Jiang, J.Z. Cui, H.L. Gao, Spectroscopic and electrochemical studies on the evaluation of the radical scavenging activities of luteolin by chelating iron, RSC Adv. 4 (2014) 25227–25233, https://doi.org/10.1039/c4ra01396d.
[22] H. Hossein-Nejad-Ariani, E. Althagafi, K. Kaur, Small peptide ligands for targeting EGFR in triple negative breast cancer cells, Sci. Rep. 9 (2019) 1–10, https://doi.org/10.1038/s41598-019-38574-y.
[23] R. Dent, M. Trudeau, K.I. Pritchard, W.M. Hanna, H.K. Kahn, C.A. Sawka, L. A. Lickley, E. Rawlinson, P. Sun, S.A. Narod, Triple-negative breast cancer: clinical features and patterns of recurrence, Clin. Cancer Res. 13 (2007) 4429–4434, https://doi.org/10.1158/1078-0432.CCR-06-3045.
[24] T.O. Nielsen, F.D. Hsu, K. Jensen, M. Cheang, G. Karaca, Z. Hu, T. Hernandez-Boussard, C. Livasy, D. Cowan, L. Dressler, L.A. Akslen, Immunohistochemical and clinical characterization of the basal-like subtype of invasive breast carcinoma, Clin. Cancer Res. 10 (2004) 5367–5374, https://doi.org/10.1158/1078-0432.CCR-04-0220.
[25] V. Secq, J. Villeret, F. Fina, M. Carmassi, X. Carcopino, S. Garcia, I. Metellus, L. Boubli, J. Iovanna, C. Charpin, Triple negative breast carcinoma EGFR amplification is not associated with EGFR, Kras or ALK mutations, Br. J. Cancer 110 (2014) 1045–1052, https://doi.org/10.1038/bjc.2013.794.
[26] Y. Tang, L. Zhu, Y. Li, J. Ji, J. Li, F. Yuan, D. Wang, W. Chen, O. Huang, X. Chen, J. Wu, Overexpression of epithelial growth factor receptor (EGFR) predicts better response to neo-adjuvant chemotherapy in patients with triple-negative breast cancer, in: J Translational Medicine, vol. 10, BioMed Central, 2012, https://doi.org/10.1186/1479-5876-10-S1-S4.
[27] K.A. Totaro, X. Liao, K. Bhattacharya, J.I. Finneman, J.B. Sperry, M.A. Massa, J. Thorn, S.V. Ho, B.L. Pentelute, Systematic investigation of EDC/sNHS-mediated bioconjugation reactions for carboxylated peptide substrates, Bioconjugate Chem. 27 (2016) 994–1004, https://doi.org/10.1021/acs.bioconjchem.6b00043.
[28] F. Li, H. Xia, Dopamine-functionalized poly (vinyl alcohol) elastomer with melt processability and self-healing properties, J. Appl. Polym. Sci. 134 (2017), 45072, https://doi.org/10.1002/app.45072.
[29] C.Y. Lin, C.H. Liu, W.L. Tseng, Fluorescein isothiocyanate-capped gold nanoparticles for fluorescent detection of reactive oxygen species based on thiol oxidation and their application for sensing glucose in serum, Anal. Methods 2 (2010) 1810–1815, https://doi.org/10.1039/C0AY00428F.
[30] T. Mosmann, Rapid colorimetric assay for cellular growth and survival: application to proliferation and cytotoxicity assays, J. Immunol. Methods 65 (1983) 55–63, https://doi.org/10.1016/0022-1759(83)90303-4.
[31] A. Halder, M. Jethwa, P. Mukherjee, S. Ghosh, S. Das, A.B.M. Helal Uddin, A. Mukherjee, U. Chatterji, P. Roy, Lactoferrin tethered betulinic acid nanoparticles promote rapid delivery and cell death in triple negative breast and laryngeal cancer cells. Artificial Cells, Nanomed. Biotech. 48 (2020) 1362–1371, https://doi.org/10.1080/21691401.2020.1850465.
[32] A. Halder, P. Mukherjee, S. Ghosh, S. Mandal, U. Chatterji, A. Mukherjee, Smart PLGA nanoparticles loaded with Quercetin: cellular uptake and in-vitro anticancer study, Mater. Today Proc. 5 (2018) 9698–9705, https://doi.org/10.1016/j.matpr.2017.10.156.
[33] G. Cravotto, P. Cintas, Forcing and controlling chemical reactions with ultrasound, Angew. Chem. Int. Ed. 46 (2007) 5476–5478, https://doi.org/10.1002/anie.200701567.
[34] D. Cristea, I. Bareau, G. Vilarem, Identification and quantitative HPLC analysis of the main flavonoids present in weld (Reseda luteola L.), Dyes Pigments 57 (2003) 267–272, https://doi.org/10.1016/S0143-7208(03)00007-X.
[35] S.F. Nabavi, N. Braidy, O. Gortzi, E. Sobarzo-Sanchez, M. Daglia, K. Skalicka-Woźniak, S.M. Nabavi, Luteolin as an anti-inflammatory and neuroprotective agent: a brief review, Brain Res. Bull. 119 (2015) 1, https://doi.org/10.1016/j.brainresbull.2015.09.002.
[36] C.E. Aruwa, S.O. Amoo, N. Koorbanally, T. Kudanga, Enzymatic dimerization of luteolin enhances antioxidant and antimicrobial activities, Biocatal. Agric. Biotechnol. 35 (2021), 102105, https://doi.org/10.1016/j.bcab.2021.102105.
[37] Y.T. Huang, J.J. Hwang, P.P. Lee, F.C. Ke, J.H. Huang, C.J. Huang, C. Kandaswami, E. Middleton, M.T. Lee, Effects of luteolin and quercetin, inhibitors of tyrosine kinase, on cell growth and metastasis-associated properties in A431 cells overexpressing epidermal growth factor receptor, Br. J. Pharmacol. 128 (1999) 999–1010, https://doi.org/10.1038/sj.bjp.0702879.
[38] M. Imran, A. Rauf, T. Abu-Izneid, M. Nadeem, M.A. Shariati, I.A. Khan, A. Imran, I. E. Orhan, M. Rizwan, M. Atif, T.A. Gondal, Luteolin, a flavonoid, as an anticancer agent: a review, Biomed. Pharmacother. 112 (2019), 108612, https://doi.org/10.1016/j.biopha.2019.108612.
[39] P. Riesz, Free radical generation by ultrasound in aqueous solutions of volatile and non-volatile solutes, Adv. Sonochem. 2 (1991) 23–64.
[40] G. Frens, Controlled nucleation for the regulation of the particle size in monodisperse gold suspensions, Nat. Phys. Sci. (Lond.) 241 (1973) 20–22, https://doi.org/10.1038/physci241020a0.
[41] S. Biggs, P. Mulvaney, C.F. Zukoski, F. Grieser, Study of anion adsorption at the gold-aqueous solution interface by atomic force microscopy, J. Am. Chem. Soc. 116 (1994) 9150–9157, https://doi.org/10.1021/ja00099a033.
[42] F. Wang, V.N. Richards, S.P. Shields, W.E. Buhro, Kinetics and mechanisms of aggregative nanocrystal growth, Chem. Mater. 26 (2014) 5–21, https://doi.org/10.1021/cm402139r.
[43] M. Tran, R. DePenning, M. Turner, S. Padalkar, Effect of citrate ratio and temperature on gold nanoparticle size and morphology, Mater. Res. Express 3 (2016), 105027, https://doi.org/10.1088/2053-1591/3/10/105027.
[44] J.H. Lee, S.U. Choi, S.P. Jang, S.Y. Lee, Production of aqueous spherical gold nanoparticles using conventional ultrasonic bath, Nanoscale Res. Lett. 7 (2012) 1–7, https://doi.org/10.1186/1556-276X-7-420.
[45] A. Halder, S. Das, T. Bera, A. Mukherjee, Rapid synthesis for monodispersed gold nanoparticles in kaempferol and anti-leishmanial efficacy against wild and drug resistant strains, RSC Adv. 7 (2017) 14159–14167, https://doi.org/10.1039/C6RA28632A.
[46] M. Kaszuba, D. McKnight, M.T. Connah, F.K. McNeil-Watson, U. Nobbmann, Measuring sub nanometre sizes using dynamic light scattering, J. Nanoparticle Res. 10 (2008) 823–829, https://doi.org/10.1007/s11051-007-9317-4.
[47] Y. Zhang, M. Yang, N.G. Portney, D. Cui, G. Budak, E. Ozbay, M. Ozkan, C. S. Ozkan, Zeta potential: a surface electrical characteristic to probe the interaction of nanoparticles with normal and cancer human breast epithelial cells, Biomed. Microdevices 10 (2008) 321–328, https://doi.org/10.1007/s10544-007-9139-2.
[48] P. Roy, S. Das, R.G. Auddy, A. Saha, A. Mukherjee, Engineered andrographolide nanoparticles mitigate paracetamol hepatotoxicity in mice, Pharm. Res. (N. Y.) 30 (2013) 1252–1262, https://doi.org/10.1007/s11095-012-0964-5.
[49] J.O. Bockris, W.K. Paik, M.A. Genshaw, Adsorption of anions at the solid-solution interface. Ellipsometric study, J. Phys. Chem. 74 (1970) 4266–4275, https://doi.org/10.1021/j100718a015.
[50] S. Das, P. Roy, S. Mondal, T. Bera, A. Mukherjee, One pot synthesis of gold nanoparticles and application in chemotherapy of wild and resistant type visceral leishmaniasis, Colloids Surf. B Biointerfaces 107 (2013) 27–34, https://doi.org/10.1016/j.colsurfb.2013.01.061.
[51] S. Das, A. Halder, S. Mandal, M.A. Mazumder, T. Bera, A. Mukherjee, P. Roy, Andrographolide engineered gold nanoparticle to overcome drug resistant visceral leishmaniasis, Artif. Cell Nanomed. Biotechnol. 46 (sup1) (2018) 751–762, https://doi.org/10.1080/21691401.2018.1435549.
[52] C. Berthomieu, R. Hienerwadel, Fourier transform infrared (FTIR) spectroscopy, Photosynth. Res. 101 (2009) 157–170, https://doi.org/10.1007/s11120-009-9439-x.
[53] S. Rajhard, L. Hladnik, F.A. Vicente, S. Srčič, M. Grilc, B. Likozar, Solubility of luteolin and other polyphenolic compounds in water, nonpolar, polar aprotic and protic solvents by applying FTIR/HPLC, Processes 9 (2021) 1952, https://doi.org/10.3390/pr9111952.
[54] H. Dong, X. Yang, J. He, S. Cai, K. Xiao, L. Zhu, Enhanced antioxidant activity, antibacterial activity and hypoglycemic effect of luteolin by complexation with manganese (II) and its inhibition kinetics on xanthine oxidase, RSC Adv. 7 (2017) 53385–53395, https://doi.org/10.1039/C7RA11036G.
[55] T.T. Bhattacharjee, M.L. Castilho, I.R. de Oliveira, V.P. Jesus, K.C. Hewitt, L. Raniero, FTIR study of secondary structure changes in Epidermal Growth Factor by gold nanoparticle conjugation, Biochim. Biophys. Acta, Gen. Subj. 1862 (2018) 495–500, https://doi.org/10.1016/j.bbagen.2017.11.009.
[56] M.L. Castilho, K.C. Hewitt, L. Raniero, FT-IR characterization of a theranostic nanoprobe for photodynamic therapy and epidermal growth factor receptor targets, Sensor. Actuator. B Chem. 240 (2017) 903–908, https://doi.org/10.1016/j.snb.2016.09.011.
[57] H. Masuda, D. Zhang, C. Bartholomeusz, H. Doihara, G.N. Hortobagyi, N.T. Ueno, Role of epidermal growth factor receptor in breast cancer, Breast Cancer Res. Treat. 136 (2012) 331–345, https://doi.org/10.1007/s10549-012-2289-9.
[58] N.T. Ueno, D. Zhang, Targeting EGFR in triple negative breast cancer, J. Cancer 2 (2011) 324–328, https://doi.org/10.7150/jca.2.324, 2011.
[59] K. Nakai, M.C. Hung, H. Yamaguchi, A perspective on anti-EGFR therapies targeting triple-negative breast cancer, Am. J. Cancer. Res. 6 (2016) 1609–1623. PMCID: PMC5004067.
[60] L. Huang, K. Jin, H. Lan, Luteolin inhibits cell cycle progression and induces apoptosis of breast cancer cells through downregulation of human telomerase reverse transcriptase, Oncol. Lett. 17 (2019) 3842–3850, https://doi.org/10.3892/ol.2019.10052.
[61] G.J. Crasto, N. Kartner, Y. Yao, K. Li, L. Bullock, A. Datti, M.F. Manolson, Lu inhibition of V-ATPase a3-d2 interaction decreases osteoclast resorptive activity, J. Cell. Biochem. 114 (2013) 929–941, https://doi.org/10.1002/jcb.24434.
[62] R. Raina, S. Pramodh, N. Rais, S. Haque, J. Shafarin, K. Bajbouj, M. Hamad, A. Hussain, Lu inhibits proliferation, triggers apoptosis and modulates Akt/mTOR and MAP kinase pathways in HeLa cells, Oncol. Lett. 21 (2021) 1, https://doi.org/10.3892/ol.2021.12452.

Received: 23 April 2022 | Revised: 4 July 2022 | Accepted: 22 July 2022

DOI: 10.1002/ddr.21979

REVIEW ARTICLE

DRUG DEVELOPMENT RESEARCH WILEY

A review on synthetic strategy, molecular pharmacology of indazole derivatives, and their future perspective

Suvadeep Mal[1] | Udita Malik[2] | Monalisa Mahapatra[1] | Abhishek Mishra[3] | Dilipkumar Pal[2] | Sudhir K. Paidesetty[1]

[1]Department of Pharmaceutical Chemistry, Siksha 'O' Anusandhan University (Deemed to be University), Bhubaneswar, Odisha, India

[2]Department of Pharmacy, Guru Ghasidas Vishwavidyalaya (A Central University), Bilaspur, Chhattisgarh, India

[3]Aurobindo Pharma, Morrisville, Durham, North Carolina, USA

Correspondence

Dilipkumar Pal, Department of Pharmacy, Guru Ghasidas Vishwavidyalaya (A Central University), Bilaspur 495009, Chhattisgarh, India.
Email: drdilip2003@yahoo.co.in

Sudhir K. Paidesetty, Department of Pharmaceutical Chemistry, Siksha 'O' Anusandhan University (Deemed to be University), Campus-2, Ghatikia, Kalinga Nagar, Bhubaneswar 731003, Odisha, India.
Email: psudhirkumar@soa.ac.in

Abstract

With different nitrogen-containing heterocyclic moieties, Indazoles earn one of the places among the top investigated molecules in medicinal research. Indazole, an important fused aromatic heterocyclic system containing benzene and pyrazole ring with a chemical formula of $C_7H_6N_2$, is also called benzopyrazole. Indazoles consist of three tautomeric forms in which 1*H*-tautomers (indazoles) and 2*H*-tautomers (isoindazoles) exist in all phases. The tautomerism in indazoles greatly influences synthesis, reactivity, physical and even the biological properties of indazoles. The thermodynamic internal energy calculation of these tautomers points view 1*H*-indazole as the predominant and stable form over 2*H*-indazole. The natural source of indazole is limited and exists in alkaloidal nature (i.e., nigellidine, nigeglanine, nigellicine, etc.) found from *Nigella* plants. Some of the FDA-approved drugs like Axitinib, Entrectinib, Niraparib, Benzydamine, and Granisetron are being used to treat renal cell cancer, non-small cell lung cancer (NSCLC), epithelial ovarian cancer, chronic inflammation, chemotherapy-induced nausea, vomiting, and many more uses. Besides all these advantages regarding its biological activity, the main issue about indazoles is the less abundance in plant sources, and their synthetic derivatives also often face problems with low yield. In this review article, we discuss its chemistry, tautomerism along with their effects, different schematics for the synthesis of indazole derivatives, and their different biological activities.

KEYWORDS

analgesic, anticancer, anti-inflammatory, benzopyrazole, indazole, SARs, tautomers

1 | INTRODUCTION

Nitrogen-containing heterocycles are recognized as the world's largest selling drugs just because of their flexibility toward different biological scaffolds and pharmaceutical products. Different nitrogen-containing heterocycles like indole, indazole, quinolone, quinazoline, carbazole, quinoxaline, purine, pyrimidine, antipyrine (J. Sahoo et al., 2020), norharmane (C. R. Sahoo et al., 2019), oxadiazole, thiazole (Pal et al., 2014), so on, are some of the crucial building blocks for several synthetic and semi-synthetic drugs. Among them, indazole and its derivatives had attracted many researchers over the past as it covers the broad area of medicinal and pharmaceutical activities. Indazole (**1**) (Figure 1) is a fused ring system belonging to the indole family, also known as benzpyrazole (Thangadurai et al., 2012). The fusion of the pyrazole ring with the benzene ring produces this ring system, which was first defined by scientist Emil Fisher. In the year 1883, during their research work, they found a new compound by heating o-hydrazino cinnamic acid (2) (Figure 1), Fisher and Kuzel named this compound as indazole observing the structural resemblance with indole (Gaikwad et al., 2015; Li et al., 2012). Indazole contains two nitrogen atoms in its

